Title

Viscoplastic modelling of rainfall-driven slow-moving landslides: application to California Coast Ranges

Journal

Landslides, 20(6)

ISSN

1612-510X

Authors

Li, Xiang
Handwerger, Alexander L
Buscarnera, Giuseppe

Publication Date

2023-06-01

DOI

10.1007/s10346-023-02039-1

Viscoplastic Modelling of Rainfall-driven Slow-moving Landslides: Application to California Coast Ranges

Xiang Li[1], Alexander L. Handwerger[2,3], and Giuseppe Buscarnera[1]

[1] Department of Civil and Environmental Engineering, Northwestern University, Evanston, USA

[2]Jet Propulsion Laboratory, California Institute of Technology, Pasadena, USA.

[3]Joint Institute for Regional Earth System Science and Engineering, University of California, Los Angeles, Los Angeles, USA.

ABSTRACT

Slow-moving landslides are widely observed in mountainous areas worldwide. While most of these landslides move slowly downslope over long periods of time, some ultimately accelerate rapidly and fail catastrophically. Simulating the landslide creep movement triggered by environmental factors such as precipitation, is therefore necessary to anticipate potential damaging effects on proximal infrastructure, habitat, and life. Here, we present a physically-based model that links pore-water pressure changes in the landslide mass with a new viscoplastic constitutive law designed to capture different temporal trends in slow-moving landslides. The model accounts for landslide velocity changes caused by rainfall infiltration through the Terzaghi's effective stress principle, thus directly resolving the deformation of the active shear zone. Calibration and validation of the computations benefited from both ground-based and remote sensing data for three active landslides in the California Coast Ranges, USA. We find that our model can accurately describe both slow quasi-continuous and episodic movement commonly displayed by active landslides. Although inherent limitations of the viscoplasticity framework did not enable us to describe catastrophic landslide acceleration, our model provides versatile tools that can be used to analyze and describe distinct types of slow-moving landslide dynamics.

Keywords: *slow-moving landslides, rainfall infiltration, constitutive modeling, rate-dependent strength.*

1 Introduction

Slow-moving landslides (Hungr et al., 2014) are widely observed in mountainous areas (Keefer and Johnson, 1983; Baum and Reid, 1995; Oberender and Puzrin, 2016; Lacroix, et al., 2020). These landslides can remain active for decades or centuries (Mackey et al., 2009) and often exhibit velocity variations related to local environmental changes (Corominas et al., 2005; Bennett et al., 2016; Hilley et al., 2004; Cascini et al., 2010). With velocities around 1m/year, slow-moving landslides can cause severe damage to proximal infrastructure and habitats (Mansour et al., 2011). Some of them can even transition from slow (within 1 m/year) to rapid (more than 1 m/s) displacement and lead to significant damage and even fatalities (Hendron and Patton, 1985; Li et al., 2020). It is therefore of great importance to interpret the velocity change of slow-moving landslides in order to manage the potential damage.

Slow-moving landslides are commonly driven by pore-water pressure transients that can result from infiltrating precipitation. When infiltration occurs, the pore-water pressures rise and cause a decrease in the normal stress applied on the landslide material (Terzaghi, 1925). Consequently, the resistance to downslope sliding is diminished and this can trigger the activation or acceleration of the landslide. Thus, hydrologic models have been developed to compute precipitation-induced pore-water pressures within the landslide body and can be used to explain observed landslide velocity variations (Iverson, 2000; Van Asch et al., 1996; Baum, 2000; Cohen-Waeber et al., 2018). Unsaturated effects from the local vadose zone (Finnegan et al., 2021) and flow induced particle redistribution (Wang and Sassa, 2003; Cui et al., 2019) have also been shown to play an important role in controlling the onset of landslide motion. In addition, the flow-deformation coupling effects on landslides dynamics have been taken into account (Iverson, 2005), showing

that the shear zone volumetric deformation (in dilation or contraction) determines whether a landslide will exhibit steady movement or runaway acceleration.

In addition to hydrological effects, the material mechanical properties will also influence the landslide behaviors. Earthen materials normally exhibit time-dependent behaviors such as creep, relaxation, and rate-sensitivity (Augustesen et al., 2004; Tika et al., 1996; Scaringi et al., 2018). Such properties often influence the mobility of landslides and can be computed through rate-dependent strength models based on viscoplasticity (Mitchell et al., 1968; Liingaard et al., 2004; Marinelli et al., 2018). It is found that the strength of earthen materials can evolve if the shear rates vary from low (within 1 m/year) to high (more than 1m/s) (Alonso et al., 2016; Scaringi et al., 2018). Under low shear rates, earthen materials normally exhibit rate-strengthening (Rice et al., 2001; Wedage et al., 1998); while high shear rates can induce rate-weakening (Di Toro et al., 2006; Mizoguchi et al., 2007). A recent study of the Two Towers landslide, northern California (study area of this paper) indicated that the shearing resistance is invariant under the range of sliding rates exhibited in the field (Schulz et al, 2018). Yet, the ring shear tests used to characterize the Two Towers landslide material showed the friction angle varies between ~21° and ~24° with shear rates from 0.01 to 1 mm/s (both rate weakening and rate strengthening were observed in this range). Such changes, although small, indicate some degree of rate-dependent behavior, which can be characterized with viscoplasticity (e.g., Mitchell et al., 1968).

Viscoplasticity has been used widely to quantify the creeping movement of landslides in response to precipitation (Angeli et al., 1996; Van Asch et al, 2007; Oberender and Puzrin, 2016; Conte et al., 2014). Viscoplastic models are able to describe a variety of slow-moving landslide behaviors and have additional modeling benefits because they ensure stable computations of landslide creeping under quasi-static conditions (i.e., no runaway instability of the landslide mass) (Perzyna,

1963; Needleman, 1988). Despite earthen material viscosity can be limited, which may prevent them from accurately describing some of the mechanisms that govern the landslide behavior (Schulz et al, 2018; Iverson, 2020), they can be used to quantify the landslide creep movement accurately.

In this manuscript, we develop a hybrid rate-strengthening rheological law able to account for pre-yield plastic deformation, which we argue is a key component of landslide deformation commonly missing in landslide models (di Prisco and Imposimato, 1997; Zambelli et al., 2004; Shi et al., 2018), that can describe the continuous and episodic movements exhibited by slow-moving landslides. This rheological model is used in conjunction with the 1D infinite slope model (Skempton and Lory, 1957) and a hydrologic framework to simulate rainfall infiltration (Lizarraga and Buscarnera, 2018). The paper is outlined as follows: first, we describe the features of the numerical model. Then, we test our formulation by simulating simple monotonic and cyclic pore water pressure variations that enable us to better constrain the impact of each model parameter. Finally, our model is applied to capture the movement of three active landslides in the California Coast Ranges, USA.

2 Model description

2.1 Landslide and hydrologic model

Our landslide model is constructed in accordance with a 1D infinite slope geometry and has three components (Fig. 1): (1) a thick, rigid landslide body, (2) a thin deforming shear zone, and (3) undeforming stable material (e.g., bedrock) below the moving mass. This landslide model geometry is based on evidence from numerous field studies that have shown that the thickness of slow-moving landslides is a few meters to tens of meters, while the thickness of the shear zone

varies from few centimeters to several tens of centimeters (Corominas et al., 2000; Leroueil, 2001; Puzrin and Schmid, 2011; Schulz et al., 2018).

We simulate pore-water pressure (p_w) changes inside a saturated landslide using a hydrologic model that is designed to solve a mass balance equation (Eq. 1) (Richards, 1931). Here we ignore the nonlinear effects that stem from unsaturated conditions (Yeh and Ward, 1980), which implies that the nonlinear functions that describe soil-water interactions in the vadose zone (i.e., Water Retention Curve and Hydraulic Conductivity Function) are encapsulated into two constants, namely the storage coefficient, S_s, and the saturated permeability, k_s. This simplification leads to a linear diffusion equation that has been widely used for simple pore-water pressure simulations in landslide studies (e.g., Iverson 2000; Cohen-Waeber et al., 2018; Berti and Simoni 2010). The change in pore-water pressure can be computed through

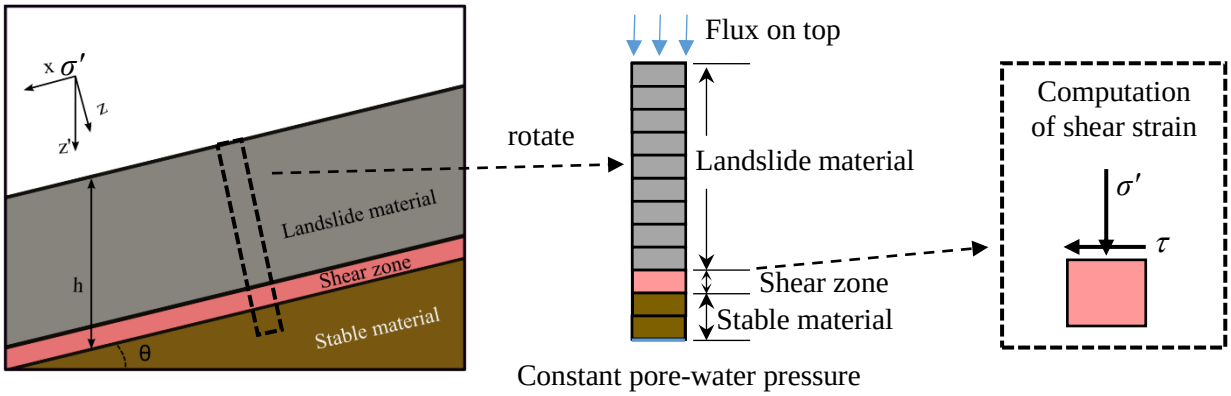

Figure 1. Schematic of the infinite slope model, along with the corresponding boundary conditions and shear strain computation at the reference shear zone element used for the simulations. The schematic is not to scale. The thickness of the landslide material, depth of the shear zone, and slope inclination θ of each case study are described later in Section 5.

$$S_s \frac{\partial h_w}{\partial t} = \frac{\partial}{\partial z}\left(k_s \frac{\partial (h_w + z)}{\partial z}\right), \quad (1)$$

where z is the normal distance from the ground surface, h_w is water pressure head (pore-water pressure p_w divided by the unit weight of water). This partial differential equation is solved

115 through the algorithm proposed by Lizárraga and Buscarnera (2018), which enables a
116 straightforward incorporation of permeability contrasts. The latter feature is useful to account for
117 permeability changes between the landslide body, shear zone, and stable ground (Baum and Reid,
118 1995).

119 Nereson et al. (2018) examined the differences in permeability within the Oak Ridge landslide,
120 central California. Their results indicated that the shear zone permeability is around two orders of
121 magnitude lower than the overlying landslide material, while the stable material below the
122 landslide shear zone has a permeability around two times higher than the landslide material. All
123 case studies in this manuscript are located in the same geological unit (Franciscan Complex
124 mélange) as the Oak Ridge landslide. Thus, we adopt this stratigraphic framework for our model
125 simulations. We set the saturated permeability of the three components (Fig. 1) in our model (the
126 ratios between shear zone k_s, sliding material k_s, and stable material k_s are 1:0.01:0.005). The top
127 boundary condition is an imposed water flux from rainfall data. We also set a constant pore-water
128 pressure boundary condition three meters below the sliding surface allocated in the stable material,
129 which is consistent with prior observations by Iverson and Major (1987) and serves as the bottom
130 boundary in our analysis.

131 The hydrologic model is then linked to our mechanical model through the effective normal stress
132 theory. The simulated rainfall-induced changes in pore-water pressure cause changes in the
133 effective normal stress, defined as $\sigma' = \sigma - p_w$, where σ is the total normal stress at the considered
134 depth. The strain resulting from such changes in effective stress is computed through the
135 constitutive models outlined in section 2.2.

2.2 Constitutive models

Here we outline a viscoplastic flow model to describe slow-moving landslides. In our model, the inelastic deformation captures both shear strain (in the sliding direction) and normal strain (in the direction perpendicular to the slope). We apply the Mohr-Coulomb yield criterion (Coulomb, 1776):

$$f = \tau - \eta_y \sigma', \tag{2}$$

where f is the yield function, τ is the shear stress, and η_y is the stress ratio at yield. $\eta_y = \tan\varphi$, φ is material friction angle at yield. Although inelastic strains due to suction loss may play a key role in shallow landslide deformation processes (Li et al., 2021; Chen and Buscarnera, 2021), thus requiring specific constitutive laws (e.g., Alonso et al., 1990), unsaturated effects have not been taken into account in this study, in that for most landslides in the selected studied area the shear zones are below the phreatic level and, thus, fully saturated. In addition, the plastic shear strain γ^p is determined by the viscoplastic flow rule (Perzyna, 1963;1966):

$$\frac{d\gamma^p}{dt} = \phi(f)\frac{\partial g}{\partial \tau}, \tag{3}$$

where $\phi(f)$ is the viscous nucleus that controls the magnitude of the plastic strain rate. Possible expressions for these functions will be specified in the section 2.3. The direction of the viscoplastic strain rate is defined by the stress gradient of the plastic potential *g* (equals to *f* for an associated flow rule). Although the earthen material viscosity can be relatively small, and other mechanisms such as dilation or compaction-induced pore-water pressure changes may be important in controlling landslides (e.g., Iverson, 2005), this class of rheological models provide a platform that

is versatile for landslide simulations aimed at quantifying slope creep movements (Van Asch, 2007; Angeli et al., 1996; Oberender and Puzrin, 2016; Conte et al., 2014).

2.3 Rheological law

The viscous nucleus (Eq. 3), which quantifies the strain rate, is a core element of a viscoplastic rheology. Here, viscoplasticity is implemented by following the overstress approach proposed by Perzyna (1966). Such framework can be regarded as a generalization of the Bingham rheology (Bingham, 1917) for general stress states and yielding criteria. As such, this framework has been widely adopted to interpret the results of earthen material laboratory tests (Liingaard et al., 2004) and simulate landslide movement (Angeli et al., 1996; Oberender and Puzrin, 2016; Van Asch et al., 2007). Standard expressions of the viscous nucleus rely on power law functions (Van Asch et al, 2007; Marinelli et al., 2018), as follows

$$\phi(f) = \begin{cases} \mu f^{\alpha}, f \geq 0 \\ 0, f < 0 \end{cases}, \tag{4}$$

where μ and α are model parameters. The expression above converges to a Bingham-like rheology when $\alpha = 1$. In addition, by setting $\phi(f) = 0$ for $f < 0$ no viscoplastic strain rate can emerge prior to yielding, thus indicating a bilinear trend characterized by permanent deformations only if the yield criterion is surpassed ($f > 0$). However, evidence from laboratory tests suggests that this approach can be excessively restrictive for earthen materials, which exhibit time-dependency much earlier than shear failure, including in the presence of overconsolidated states (Augustesen et al., 2004; Shi et al., 2018). To better account for these effects, exponential forms have been proposed (di Prisco and Imposimato,1996) for sand:

$$\phi(f) = \mu e^{\alpha f}. \tag{5}$$

Although Eq. 5 allows non-zero pre-yielding viscosity, by letting the viscoplastic deformation gradually augment as the stress state moves away from the failure envelope, its exponential form tends to produce excessive plastic strain rate once the yield surface is surpassed. We provide an illustrative example of this in Fig. 2a for a viscous nucleus characterized by α=1. Our example shows that even a small excess of the yield threshold (only 3 kPa in our example corresponding to a water level increase of 0.3 m), the exponential law predicts a shear strain rate that is more than double the rate predicted by the Bingham-like model. To address this issue, we propose a hybrid law as a mathematical compromise able to blend the benefits of above two forms above, as follows:

$$\phi(f) = \mu \ln(1 + e^{\alpha f}) . \quad (6)$$

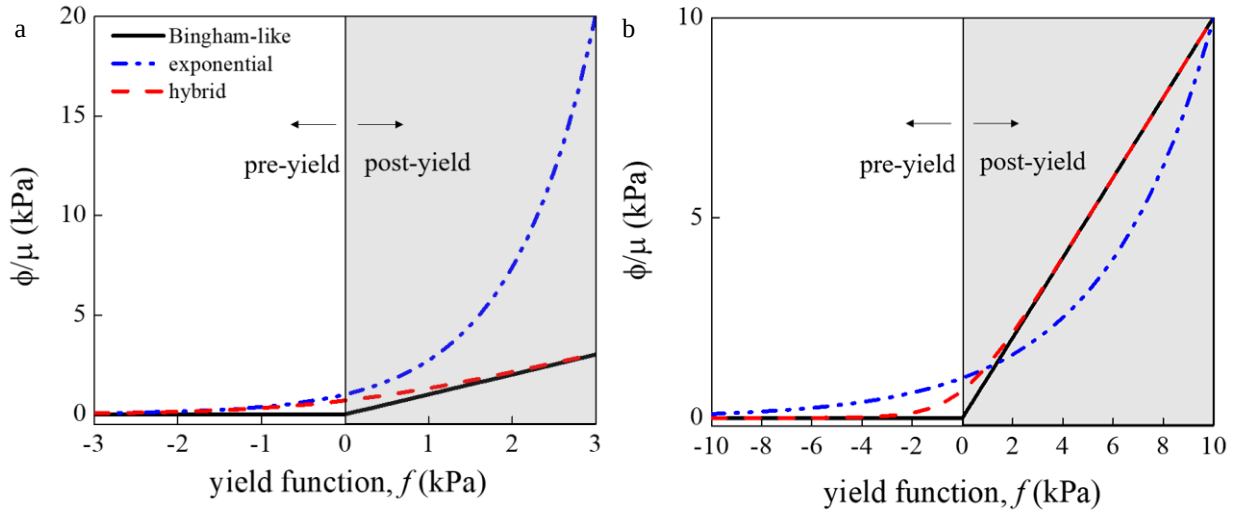

Figure 2. Factorized viscous shear strain rate (by $1/\mu$, parameter that scales the magnitude) versus yield function value for different expressions of viscous nucleus. a) Dashed-dotted blue, dashed red, and black lines show model predictions for the exponential, hybrid, and Bingham-like models with α = 1. b) Blue, dashed red, and black lines show model predictions with α = 1 for the hybrid and Bingham-like and α = 0.23 for the exponential law. These simulations show that changing the power-law rheology term can lead to the same strain rate at the maximum yield function.

Such a model can capture both pre-yield viscoplastic strain and post-yield strain rates comparable to those of widely used Bingham-like models. This effect could not have been achieved by modulating the parameters of the exponential rheology in Eq. 5 alone, because setting an ideal

strain rate at large overstress values (f =10 kPa in Fig. 2b) leads to overestimation of the strain rates in the pre-yielding regime (strain developed when f is 10 kPa). By contrast, the hybrid law we proposed enables a Bingham-like rheology to be recovered at large overstress values, while capturing slow growth (but non-zero) viscoplastic strain rates in the pre-yield regime. Thus, it can be regarded as a more versatile platform to describe the rheology of earthen materials.

2.4 Indication of pre-yield viscosity

As mentioned above, laboratory measurements have shown that earthen materials exhibit viscous properties even within the elastic domain (di Prisco and Imposimato, 1996; Sekiguchi, 1984). To test whether landslides exhibit pre-yield viscosity at the field scale, we examine relationships between measured landslide velocity and slope angle for the Boulder Creek and Mud Creek landslides in California (a detailed description of these landslides is provided in Section 4.1). The goal of this analysis is to link the landslide mobility to the stress state acting on the material, aiming at investigating if viscous effects may emerge before the material is driven into the plastic domain.

The Boulder Creek landslide has a mean ground surface slope angle of 15° and has been exhibiting quasi-steady motion (the monitored displacement over time shows nearly constant increment) for decades or longer (Handwerger et al., 2013; 2019; Mackey and Roering, 2011). The Mud Creek landslide is notably steeper with a mean ground surface slope angle of 32° and exhibited episodic motion for a minimum of 8 years before it collapsed catastrophically. We measure the average landslide velocity from a previously published surface velocity dataset (Handwerger et al., 2019). The landslide surface velocity was quantified using satellite-based interferometric synthetic-aperture radar (InSAR) data, a remote sensing technique that can measure mm- to cm-scale ground surface motion (see Section 5 for more details). We then calculate the stress ratio (shear stress/effective normal stress in nearly dry condition) using a digital elevation model (DEM,

resolution 12 m) provided by the German Space Agency (DLR). The slope angle determines the magnitude of the gravitational loading components along both normal and tangential directions (*z* and *x* displayed in Fig. 1), which effects the ratio between shear and normal stress (stress ratio). For simplicity, we assume the landslide thickness is constant and is 20 m for Mud Creek and 40 m

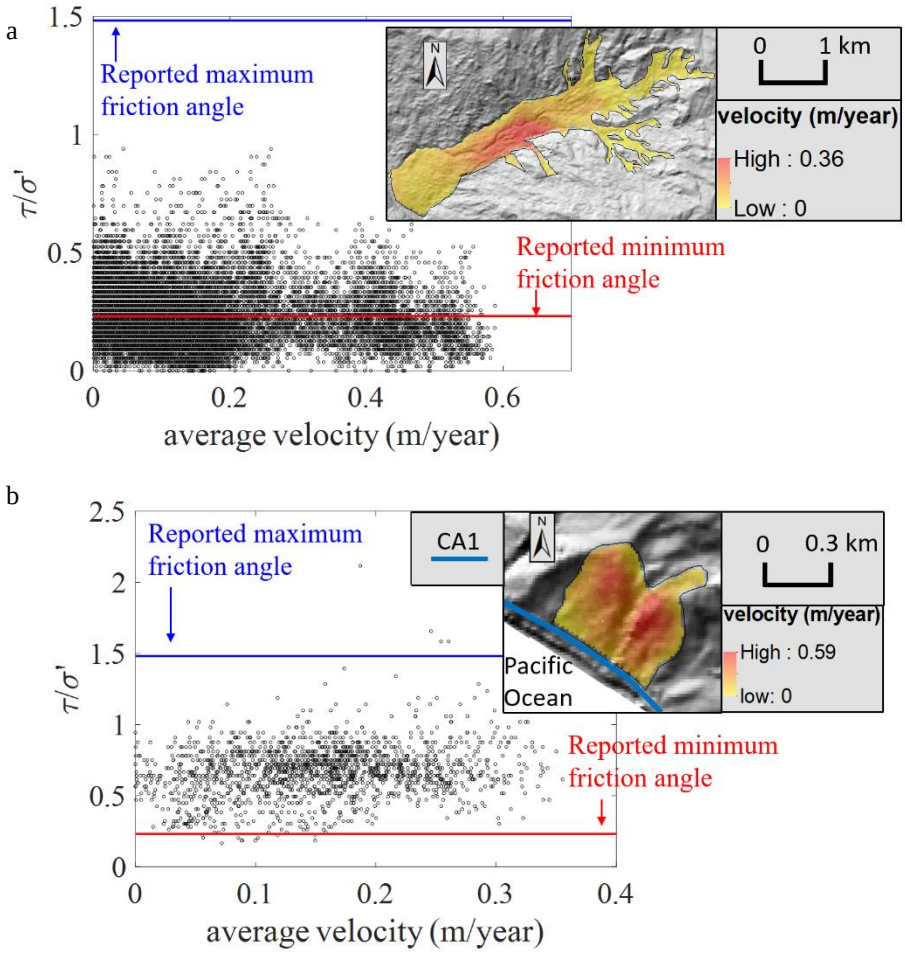

Figure 3. Pre- and post-yield motion analyses of the Boulder Creek and Mud Creek landslide. The ratio of shear stress divided by the effective normal stress vs. average velocity for a). Boulder Creek landslide, b). Mud Creek landslide. Inset images are the average downslope InSAR velocity map of each landslide plotted on top of its hillshade individually. Light blue line at base of Mud Creek shows California State Highway 1 (CA1). The data are binned by pixels with the same slope angle. Horizontal red line shows the stress ratio corresponding to 13° friction angle, which is the minimum friction angle reported by Keefer and Johnson, 1978; blue line shows the stress ratio of 56° friction angle, which is the maximum value reported by Roadifer, et al., 2009. InSAR data are from Handwerger et al. (2019) and DEM is from TanDEM-X. TanDEM-X data used is under copyright by the DLR.

for Boulder Creek (details explained in the Section 5). From classical slope stability analysis (Duncan, 1996), the relation between the stress ratio and the value at yield can indicate if the slope is predicted to be stable or unstable (the smaller the stress ratio, the further it departs from the material yield status).

Fig. 3a shows a comparison between the stress ratio and velocity for the Boulder Creek landslide. We find that for even low stress ratios, there are abundant landslide pixels that display non-negligible movement. Similarly, we compare the relation between average InSAR surface velocity and stress ratio for the Mud Creek landslide (Fig. 3b). Due to the significantly steeper slope angle, Mud Creek has a much higher stress ratio overall, but also showed some movement at low stress ratios. Geotechnical investigations (Keefer and Johnson, 1983; Schulz et al., 2018; Nereson et al., 2018) recorded that for landslide materials hosted in the Franciscan Mélange, the rock type common to both landslides, the minimum friction angle is around 13° (Keefer and Johnson, 1983) and the maximum friction angle is around 56° (Roadifer et al., 2009). Both stress ratios are depicted in Fig. 3. Our findings indicate creeping deformation occurs at stress ratios below the frictional limit and suggests the landslides exhibit a viscous material rheology in the pre-yield regime.

3 Model testing

3.1 Monotonic increase of pore-water pressure

In the previous section, factorized viscoplastic strain rates corresponding to different viscous nucleus expressions were compared. Here, to further illustrate each model's performance in response to more realistic pore-water pressure variations in landslides, all rheological laws are tested with a simulated p_w increase of 20 kPa over 180 days (i.e., a 2 m water level rise which approximates the water level change experienced by the active landslides in the California Coast

Range (Iverson and Major, 1987; Schulz et al., 2018; Finnegan et al., 2021)) directly applied to the landslide sliding surface (Fig. 4b, other parameters are listed in the figure caption). The same value of viscous parameter $\alpha = 1$ is used for all the simulations. Since the parameter μ controls the magnitude of the plastic shear strain (γ^p), here the factorized viscoplastic shear strain (γ^p/μ) is used as a basis for the model comparisons (Fig. 4a).

3.2 Sensitivity tests for hybrid model mechanical parameters

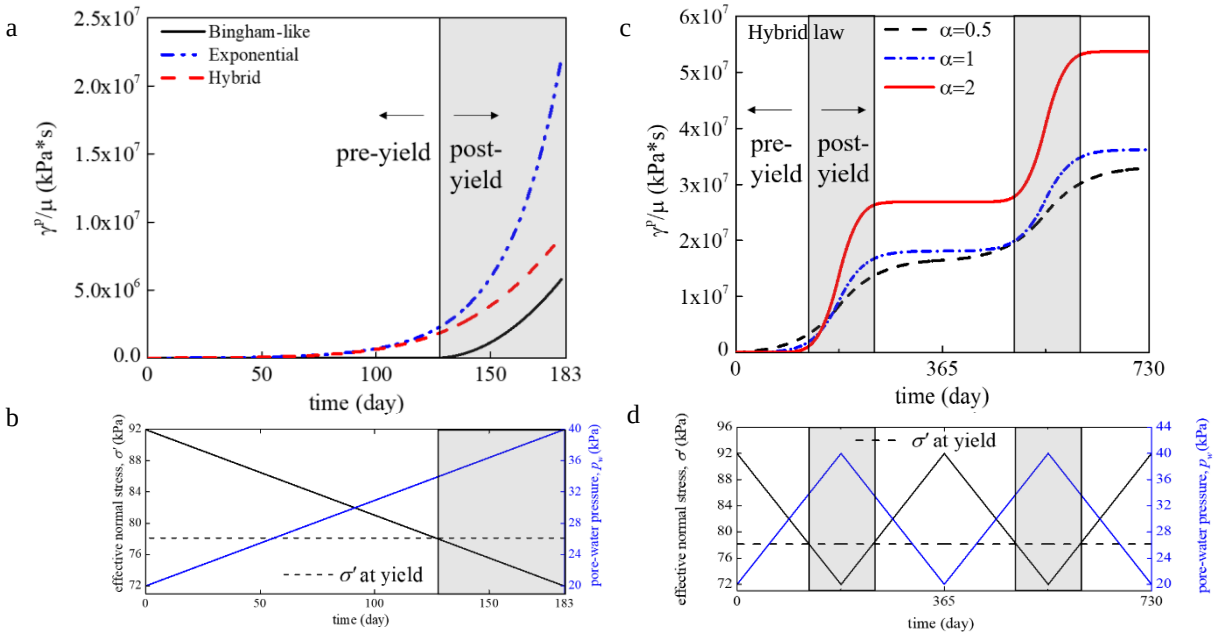

Figure 4. Comparisons of the three viscoplastic models. Shear strain is computed from rheological laws in response of monotonic increased and cyclic pore-water pressure. a) Factorized viscoplastic shear strain calculated by each rheological law. b) Pore-water pressure monotonic variation and corresponding effective normal stress. c). Factorized viscoplastic shear strain calculated Hybrid law with different value of α. d) Cyclic pore water pressure variation, corresponding effective normal stress change. For this synthetic landslide experiments the model parameters were chosen to resemble those reported for typical landslide settings in the California Coast Ranges (Schultz et al., 2018), h =6 m, θ = 15°, γ_{sat} =22 kN/m^3, φ = 21°.

Fig. 4b shows the effective normal stress variation caused by this synthetic hydraulic event. The yield surface is approached after about 130 days. Our model results show that the normalized shear strain computed from the Bingham-like model begins to increase after 130 days, while the

exponential law predicts an earlier initiation of the movement after 60 days and a predicted movement three times larger than those obtained with the Bingham law (Fig. 4a).

Our new hybrid law predicts that shear strain initiates after about 80 days, which is 50 days before the yield surface is approached, while providing total displacement at the end of the pore-water pressure growth period that is similar to those obtained from the Bingham-like model (Fig. 4a). This result confirms the ability of the proposed hybrid rheology to provide a compromise between Bingham-like models widely tested for the active stage of landslide motion and exponential formulations tailored for describing pre-yielding sliding behavior. Hereafter, parametric analyses are conducted to explore the effect of the model parameters.

The parameters of the proposed hybrid mechanical model are φ, μ and α. Among them, φ determines the pore-water pressure limit enabling episodic slips (i.e., the landslide mobilization time), while μ governs the magnitude of the displacement. α influences the sensitivity of the sliding behavior against pore-water pressure variance; as an outcome, it affects the temporal history of the sliding response in both magnitude and rate (Fig. 4c).

Fig. 4d shows another simulated pore-water pressure change and the predicted landslide response. Here we apply cyclic triangular waves of pore-water pressure of 20 kPa amplitude to approximate cyclic seasonal rainfall effects. We find that when $\alpha = 0.5$ (at 130 days), the sliding behavior prior to the stress path approaching the yield surface (50 days in advance) is discernible, while the displacement at the peak of pore-water pressure (around 180 days) is relatively small compared to the other simulations. By contrast, when $\alpha = 2$, pre-yielding effects are suppressed, and the response involves sharp episodic slips occurring only upon violation of the yield criterion. Thus, a higher α leads to marked velocity changes between periods with higher and lower pore-water pressure, which represent the wet and dry seasons commonly experienced by real landslides (e.g.,

Corominas et al., 2000). In other words, the history of the rates of landslide movement is governed by α. In the next section we will calibrate these model parameters to data from three landslides in California.

4 Case Studies

4.1 Sites of interest

Thousands of slow-moving landslides have been identified in the California Coast Ranges (Bennett et al., 2016; Handwerger et al., 2019b; Keefer and Johnson, 1983; Kelsey et al., 1995; Mackey and Roering, 2011; Scheingross et al., 2013). These landslides are widespread in this

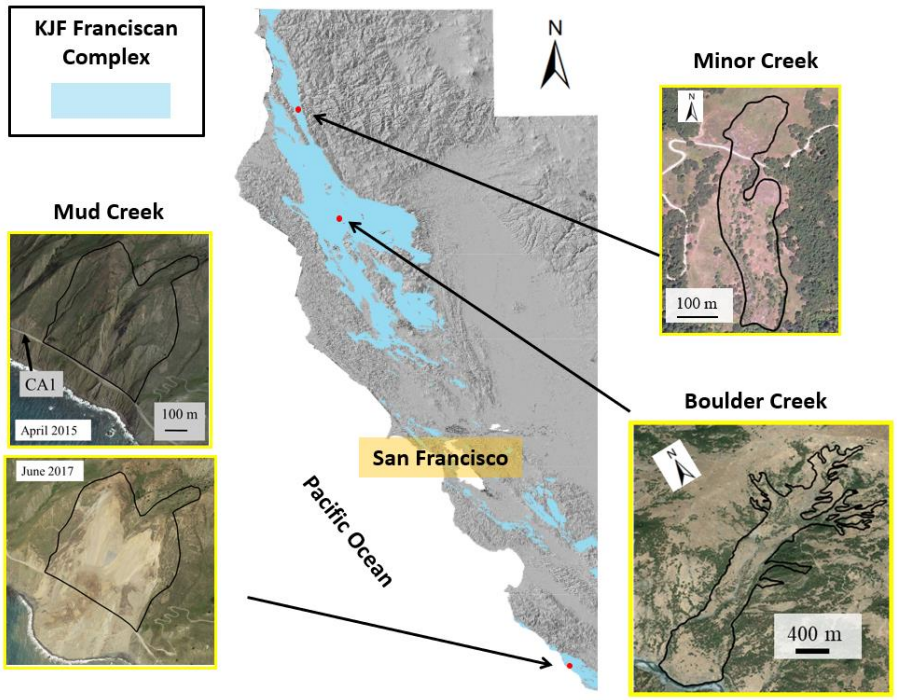

Figure 5. Landslide test sites. Northern and Central California Coast Ranges, showing the Franciscan Complex mélange unit draped over a hillshade of the topography. The hillshade was generated from a 12-m TanDEM-X DEM. The three landslide test sites used in this paper are marked on the map, along with inserts showing oblique Google Earth images . For Mud Creek landsdlie, both the images before and after catastrophic failure are shown.

region due to active tectonics, mechanically weak rocks, and high seasonal precipitation (Scheingross et al., 2013; Roering et al., 2015). The rainfall in California is seasonal with the vast

majority of precipitation occurring between October to May (Swain, 2021). Most of the landslides located within the Jurassic-Cretaceous Franciscan Mélange (KJf) (Roering et al., 2015), which is a clay-rich complex with various more resistant rocks such as sandstone, shales, serpentinite, and conglomerates (Bailey et al., 1964; Rutte et al., 2020).

Here, Minor Creek landslide, Boulder Creek landslide, and Mud Creek landslide have been selected as cases of study to test our model performance. We summarize our approach to calibrate our model in Table 1. Minor Creek was monitored between 1982-1985 using ground-based tools

Table 1. parameters calibration guidance

Model parameter	Description	Calibration from	Calibration guidance
k_s (m/s)	Saturated permeability	Pore-water pressure	Increase the value if the simulated pore pressure lags behind the measured data
S_s (m^{-1})	Storage coefficient	Pore-water pressure	Increase if the simulated pore pressure amplitude is smaller than the measured data
φ (°)	Friction angle	Movement	Decrease if the simulated sliding initiates later than observation or no sliding can be computed
α (–)	Pre- and post-yield viscosity ratio	Movement	Decrease if the movement difference in dry and wet season is larger than the measured data
μ $(kPa*s)^{-1}$	Magnitude of viscosity	Movement	Increase if the simulated sliding magnitude is smaller than the measured data

including piezometers for measuring pore-water pressure, and extensometers for monitoring displacement (see details in Iverson and Major, 1987). Mud Creek landslide and Boulder Creek landslide have no ground-based data available and instead their displacement was measured between 2015 and 2017 through satellite-based InSAR techniques (see details in Handwerger et al., 2019). Minor Creek and Boulder Creek landslides have been exhibiting slow and episodic sliding for decades or longer. Mud Creek landslide is also known to have displayed slow sliding

for more than 8 years, but this changed when it failed catastrophically on a dry day (May 20, 2017) following a prolonged period of heavy rainfall. This sudden acceleration heavily damaged the California State Highway 1 (CA1) (Fig. 5), resulting in road closure between May 2017 and July 2018 and an estimated cost of $54 million in repairs (Caltrans report, 2018). These landslides exhibit substantially different trends of movement over time; thus, they are good candidates to test the model versatility. Details of each case and correspondent model performance are discussed in the following sub-sections.

4.2 Minor Creek landslide

Minor Creek landslide (Fig. 5), a compound, complex, slow-moving landslide, covers about 10 hectares in Redwood Creek drainage basin, northern California Coast Ranges. Iverson and Major (1987) acquired three years of detailed rainfall, groundwater and movement data (Fig. 6a and 6b) of this landslide from October 1982 to September 1985. We digitized the measured rainfall and pore-water pressure based on the results shown in Fig. 10 of Iverson (2005). The average slope angle is 15°; the thickness of the landslide along its longitudinal axis is 6 m; thickness of the shear zone is around 1 m (Iverson, 1985).

The precipitation was monitored with a rain gage located at the site of the landslide, which is set as the top boundary condition of the hydraulic simulation in order to compute the rainfall induced pore-water pressure. The initial water pressure is set based on the shear zone pore-water pressure (Fig. 6a) assuming hydro-static conditions. The lower boundary condition is set as a constant pore-water pressure value three meters below the sliding surface as discussed above to reflect the observed hydrological condition that deep pore-water pressure barely changed. We calibrated our model parameters for the shear zone material using trial and error following the calibration

processes illustrated in Table 1. We found that our simulated pore-water pressure variation is consistent with the monitoring data (Fig. 6a) with the hydraulic parameters in Table 2.

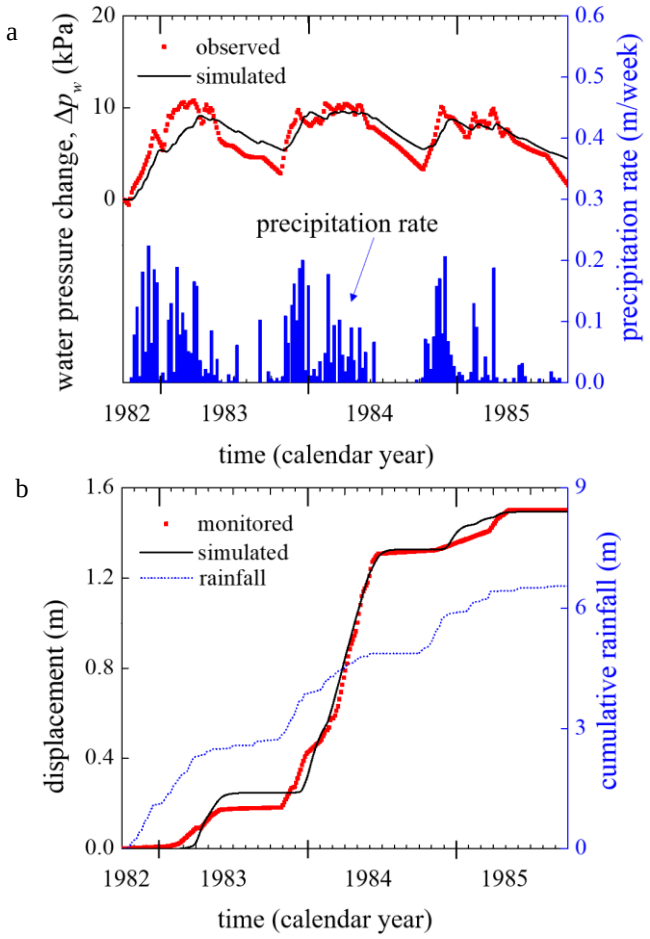

Figure 6. Pore-water pressure, rainfall, and displacement of Minor Creek landslide during 1982 ~1985. a) Monitored and simulated pore-water pressure variation at the sliding surface and the precipitation rate; b) monitored and simulated landslide movement and cumulative rainfall, model parameters shown in Table 2. Monitored data are digitized from Iverson and Major (1987).

The episodic slip movements of this landslide site (Fig. 6b) are driven by pore-water pressure changes during the wet and dry seasons. The pore-water pressure rises rapidly after onset of the wet season, remains relatively high during the wet season, and decreases slowly throughout the dry season. As a result, the landslide is barely active during the dry season and moves primarily during the wet season (Fig 6b). Such step-like episodic displacements suggest a high value of parameter α. Our best-fit model parameters are $\alpha = 8$, $\mu = 2.1 \times 10^{-8}$ (kPa*s)$^{-1}$, and friction angle (φ)

around 19° (Table 2). Fig. 6b illustrates that the landslide movement of Minor Creek landslide can be simulated accurately by our new proposed hybrid rheological model.

Table 2. model parameters for the selected case studies

Model parameters	Minor Creek	Boulder Creek	Mud Creek
k_s (m/s)	4.45E-6	4.6E-6	4.6E-6
S_s (m^{-1})	0.27	0.03	0.07
α (–)	8.00	0.15	0.70
μ $(kPa*s)^{-1}$	2.1E-8	2.1E-8	2.1E-8
φ (°)	18.9	26.1	48.5

Importantly, the model captures the relatively large displacement displayed by Minor Creek from the end of 1983 to the beginning of 1984 and the smaller displacements in the other wet seasons. This large displacement was caused by a pore-water pressure change that approaches its highest value (~10 kPa) for more than half of the year (Fig. 6a). The longer period with higher pore-water pressure leads to the apparent active landslide movement (around 1 m/year, still categorized as a slow landslide by Hungr (2014)). The results show some mismatches between our pore-water pressure and displacement simulations and the monitoring data, such as, predicting lower pore-water pressures during the wet season of water year 1983; simulating higher pore-water pressures at each dry season compared with the monitoring data; obtaining delayed, higher magnitude movement in the first year. Despite these differences, the overall agreement between our computed results and the field data corroborates the model's ability to describe both hydraulic and mechanical behavior in monitored landslides.

4.3 Boulder Creek landslide

Boulder Creek landslide (Fig. 5), northern California Coast Ranges, has displayed stable sliding for decades (Mackey and Roering, 2011). Although no ground-based monitoring of deformation or pore-water pressure is available at the site, surface movements from January 2016 to October 2017 (Fig. 7b) were measured by Handwerger et al. (2019) via InSAR images acquired by the Copernicus Sentinel-1 A/B satellites. The InSAR data show that the landslide exhibits a nearly constant displacement rate (quasi-continuous slow creeping with minor seasonal variations), thus with a temporal trend departing considerably from the episodic motion discussed previously. The average inclination of this landslide is around 15°, the area is around 310 hectares (Handwerger et al., 2013), and the estimated thickness is 40 m (Mackey and Roering, 2011). We simulated the pore-water pressure time history at the landslide base by assuming a nearly saturated initial condition. We assume saturated conditions in that field data from other landslide sites in the KJf show that the groundwater table remains within 2-3 m of the ground surface during the dry season and rises to the ground surface during the wet season (Iverson and Major, 1987; Schulz et al., 2018; Hahm et al., 2019; Finnegan et al., 2021). We used precipitation data (Fig. 7) acquired by National Oceanic and Atmospheric Administration (NOAA) as the surface boundary condition (around 50 km from the landslide). The hydrological parameters (Table 2) are back calculated as described in the Appendix. 1, where the reason that leads to different hydrological parameters for each case is also explained.

The computed pore-water pressure changes for Boulder Creek are shown in Fig. 7a. We used the same viscosity parameter μ for Minor Creek here but in order to better capture the quasi-continuous motion of Boulder Creek we had to reduce the rheological parameter α to 0.15 (section 3.2 and Table 1). We then back-calculated the friction angle φ and found a value around 26° (see

Table 2) leads to satisfactory results in a form of continuous creep deformation (Fig. 7b). Our model is able to reproduce the overall landslide displacement of Boulder Creek after making these parameter adjustments.

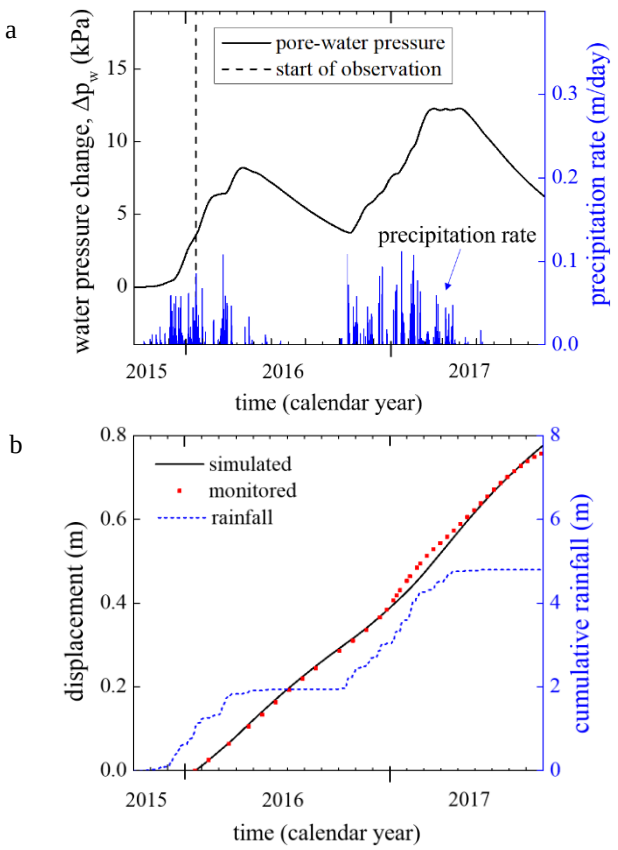

Figure 7. Pore-water pressure change, rainfall, and displacement of Boulder Creek landslide during 2015 ~2017. a) Pore-water pressure variation at sliding surface and the precipitation rate; b) monitored and simulated landslide movement time history and the cumulative rainfall, model parameters shown in Table 2.

4.4 Mud Creek landslide

Finally, we tested our model's ability to capture the slow and episodic motion displayed by the Mud Creek landslide prior to its catastrophic collapse (Fig. 5). We modeled the period of slow-motion between February 28, 2015, and May 13, 2017, that was measured with InSAR data (see details in in Handwerger et al., 2019). The landslide has an area of around 23 hectares prior to catastrophic failure, thickness of 20 m (measured after landslide collapse; see Warrick et al., 2019),

and average slope 32° (Warrick et al., 2019; Handwerger et al., 2019). Similar to the previous case, pore-water pressure changes (Fig. 8a) are simulated with the hydraulic model calibrated based on the procedures discussed in the Appendix. 1. Precipitation data from a rain-gauge (Fig. 8) located around 50 km from the landslide provided by the California Climate Data Archive were used as the surface boundary condition.

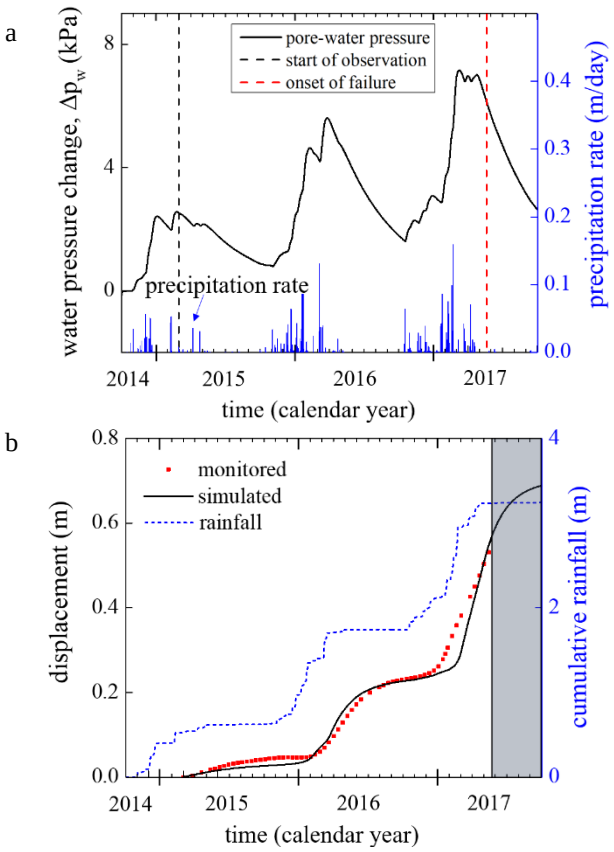

Figure 8. Pore-water pressure change, rainfall, and displacement of Mud Creek landslide during 2014 ~2017. a) Simulated pore pressure variation at sliding surface and the precipitation rate. b) Simulated landslide movement time history and measured cumulative rainfall. The left boundary of the shaded rectangle represents the occurrence of catastrophic acceleration. Our model is not able to capture runaway instability and predicts a return to slow motion (black line inside gray shaded region).

We find that our hybrid rheological model can overall predict the landslide behavior using a value of α =0.7, which is between those used for the Minor Creek and the Boulder Creek sites. Notably, we find that the back-calculated friction angle value is around 49°. This high value is because Mud

Creek is steep and thick (i.e., high initial stress ratio), and initial water level located near the ground surface (leads to high pore-water pressure). In this context, the initial basal pore-water pressure computed from stationary flow condition within an infinite slope is around 140 kPa, which is higher than typical conditions observed at other sites and used in soil laboratory testing. In fact, with an initial pore-water pressure around 20 kPa (induced by a water level around 2 m above the sliding surface) as monitored from shallower landslides located in KJf (Finnegan et al., 2021; Iverson and Major, 1987; Schulz et al., 2018), a much smaller friction angle would be back-calculated (around 34°). Further validation of this value is provided in the Discussion section.

Although our model cannot describe the runaway acceleration of the landslide, we allowed our simulations to continue to show what our model would have predicted for Mud Creek. Fig. 8b shows that a deceleration are predicted after May 20, when catastrophic runaway acceleration occurred. We show this to highlight a key limitation of our model framework and we outline plans to improve this model in the future in the Discussion section below.

5 Discussion

In this paper, we developed a new model to describe the motion of slow-moving landslides driven by precipitation. Our new model incorporates landslide activation under both pre-yield and post-yield scenarios, which is an advance over commonly used viscoplastic models. The model can be used to describe distinct types of landslide motion from episodic to quasi-stable sliding movements with simple parameter calibration.

Viscoplastic models have been used to interpret landslide creeping movement broadly. Most previous studies have used a Bingham-like rheological law (Fernandez-Merodo et al., 2014; Oberender and Puzrin, 2016), which ignores the viscous creeping before the material yield surface

is approached. However, earthen materials are found to experience viscosity under the elastic domain (di Prisco and Imposimato, 1996; Sekiguchi, 1984), and therefore models need to account for this non-negligible deformation. Our analysis based on the InSAR data also suggested that some of the areas within active slow-moving landslides were creeping even when materials were in this elastic regime. With this motivation, we developed a new Hybrid rheological model (Eq. 6) to account for the deformations. Most notably, taking pre-yield viscosity into account can significantly improve simulation of landslide movement. To show the model improvement when taking pre-yield viscosity into account, the Boulder Creek and Mud Creek landslides (where pre-yield movement are observed as explained) are selected to run computations with the three rheological laws. The calibrated parameters (Table 3) are similar for each case using different model.

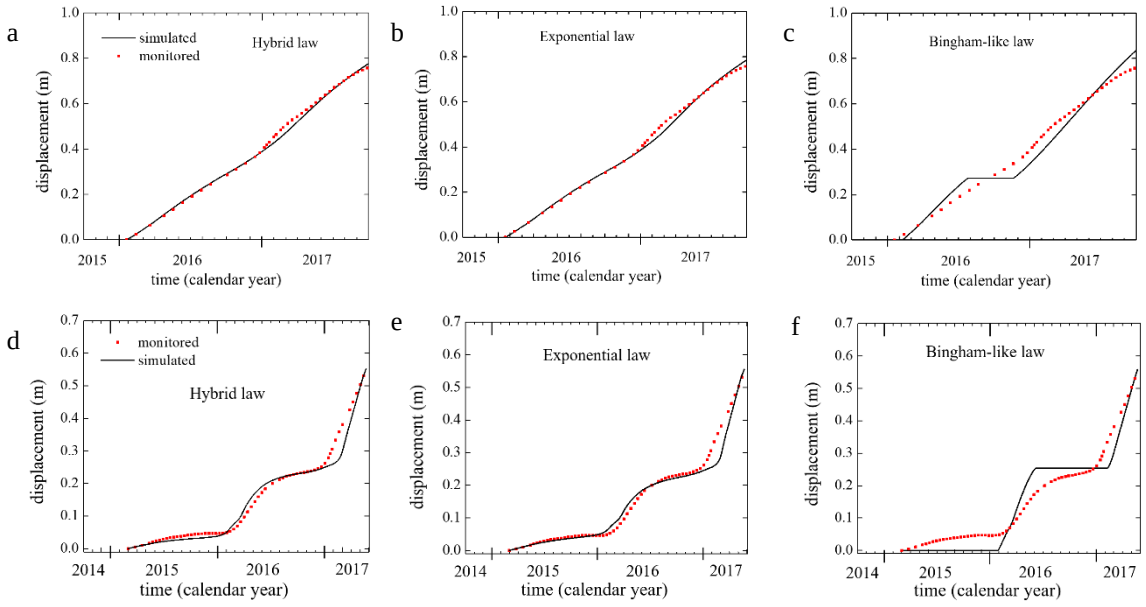

Figure. 9 Comparison of the Simulation of Boulder Creek and Mud Creek landslides using different rheological models. Boulder Creek displacement simulated using Hybrid law (a), exponential law (b), and Bingham-like law (c). Mud Creek simulated using Hybrid law (d), Exponential law (e), and Bingham-like law (f).

Fig. 9a~b and 9d~e shows that, models using the exponential and Bingham rheological laws can capture both Mud Creek and Boulder Creek landslide creep movement satisfactorily. However, if

467 the Bingham-like law is used, then during the dry season the simulated landslide stops moving,
468 which does not agree with the monitored displacement (Fig. 9c and Fig. 9f). In these case studies,
469 both our hybrid rheology and the exponential rheology can lead to accurate results within the
470 simulated periods of time. However, when dealing with higher subsequent precipitation, the
471 exponential law will lead to much higher acceleration compared to our rheological model. The
472 field observations show that annual maximum velocity of slow-moving landslide in our studied
473 area varied insignificantly (Handwerger et al., 2013). Therefore, our hybrid model can be a better
474 candidate to simulate earthen material behaviors.

475 **Table 3**. **Model parameters**

Model parameters	Hybrid (Boulder)	Exponential (Boulder)	Bingham-like (Boulder)	Hybrid (Mud)	Exponential (Mud)	Bingham-like (Mud)
α (–)	0.15	0.10	0.05	0.70	0.50	0.57
μ (kPa*s)$^{-1}$	2.1E-8	2.1E-8	2.1E-8	2.1E-8	2.1E-8	2.1E-8
φ (°)	26.1	26.5	26.0	48.5	48.7	48.3

476

477 We found that back-calculated friction angle values were higher, especially for Mud Creek, than
478 those typically reported from lab measurements at landslide sites in KJf (Keefer and Johnson,
479 1983; Iverson, 2005; Schulz et al., 2018). Our back-calculated friction values differ from these lab
480 values for a few reasons. First, the back-calculated values account for large variations in landslide
481 material properties at the field-scale known to the KJf. In fact, in lab tests by Roadifer et al., 2009,
482 which measured the friction angle as a function of block-in-matrix percent, showed that the friction
483 angle ranged from 20 to more than 50 degrees, increasing as the block-in-matrix proportion
484 increased. Second, high friction angles are required to maintain force balance when there are steep

slopes, large landslide thickness, and high assumed pore-water pressures (e.g., Mud Creek). In clay-rich slopes relatively high values of back-calculated friction angle may also partly reflect the consolidation history of the material and the consequent nonlinearity of its strength envelope (Shi et al., 2017). Lastly, we assumed that the landslide shear zone material had zero cohesion. This assumption is reasonable because most of the earthen materials from landslide shear zones have experienced significant displacement, which are likely to have rendered cohesive strength contributions negligible. However, if the material has non-negligible cohesion, this would in part offset the friction angle strength needed to maintain force balance.

Our computational process is data-driven, which means that one site of parameters from a case study cannot be used directly to other cases although the landslide materials are located in the same geological unit (KJf). It is not a surprising result as the landslides are distinct from the viewpoint of topography, average slope angle (15° to 38°); and depth of sliding surface (6-40 m). Some local conditions are also distinct site by site, such as the landslide size (Handwerger et al., 2013; Keefer and Johnson, 1983) and rainfall conditions. In addition, the KJf material properties can also be substantially different (Keefer and Johnson, 1983; Nereson, 2018).

One of the major benefits of predicting the landslide movement using viscoplastic models is that they can describe post-failure landslide motions. This provides an advantage over most elastoplastic models which lack unique solutions in post-failure scenarios (e.g., Puzrin, 2012), thus cannot be used to quantify landslide creep movement behaviors. However, several studies have shown that the viscosity of some slow-moving landslide materials is negligible, especially under the small dynamic range of motion exhibited by slow-moving landslides (e.g., Schulz et al., 2018; Iverson, 2020). Further complicating the issue, there is often a large discrepancy (more than three orders of magnitude) between viscosity values obtained from laboratory tests and the ones gathered

from case study parameter back calculations (Angeli et al., 1996; Van Asch et al., 2007). These large differences make it challenging to develop models with predictive capabilities. These prior studies indicate that viscosity might not be solely sufficient to interpret slow-moving landslide behaviors. There are other considerations that can result in rate-dependent properties and therefore be used to describe post-failure motion such as thermo-mechanical interactions (Alonso et al., 2016; Veveakis et al., 2007) and shear dilatancy (Hutchinson, 1986; Iverson et al., 2005; Chen and Buscarnera, 2022), which are not considered in this paper. In reality all of these factors may be important in controlling the landslide behavior.

Given these discrepancies, we suggest that the viscoplastic parameters back calculated for field data may be more relevant than those measured on small lab samples. In addition, the permeability of material from Minor Creek landslide (Iverson and Major, 1987) varied across 5 orders of magnitude from $1.6x10^{-5}$ to $3x10^{-10}$ m/s also suggested to back calculate this parameter from the range to capture the overall field-scale landslide behaviors.

6 Conclusions

Here we present a new model framework to simulate both the changes in subsurface pore-water pressure driven by precipitation and the dynamics of slow-moving landslides. Our hydrological model accounts for water mass diffusion across heterogeneous slope profiles. Similar to previous work, we found that our simple 1D diffusion model can capture pore-water pressure variations that are consistent with ground-based monitoring data.

We then used our hydrologic simulations as an input to drive our landslide model. We simulated the sliding behavior of three real landslides using a new hybrid viscoplastic model. We found that a hybrid viscous nucleus combined the benefits of a post-yield Bingham-like rheology that is

commonly used to model landslides, and a pre-yield creep that can describe precursory landslide deformation. Our results show that the hybrid rheology is able to capture a variety of delayed landslide movements observed at the three landslide sites in the California Coast Range. Although a complete assessment of spontaneous transitions to catastrophic acceleration requires some other factors such as thermo-mechanical interactions, progressive coalescence of discrete failure surfaces, or a fully coupled hydro-mechanical formulation, which are not addressed in this work. The analyses discussed here provide a versatile strategy to interpret velocity changes in creeping landslides governed by rainfall by incorporating explicitly both the hydraulic and mechanical effects responsible for their manifestation, thus offering a springboard for future extensions including coupled pore-water pressure feedbacks and post-failure dynamics.

ACKNOWLEDGEMENTS

This work was supported by Grant No. ICER-1854951 awarded by the U.S. National Science Foundation. Topographic data are provided by the German Aerospace Center (DLR) under data proposal DEM GEOL1478 awarded to A. L. H. To acquire these data, proposals may be submitted to the DLR online (https://tandemx-science.dlr.de/). Part of this research was carried out at the Jet Propulsion Laboratory, California Institute of Technology, under a contract with the National Aeronautics and Space Administration (80NM0018D0004).

Appendix. Back calculation of the hydraulic parameters for Boulder Creek and Mud Creek Landslides

Since there is no ground-based monitoring of pore-water pressure changes for Boulder Creek and Mud Creek landslides, we modeled the hydraulic response based on observations from the Minor Creek site. To do this, we assumed that the sliding surface of three studied cases each experienced similar hydrological changes driven by rainfall. Our assumption is justified based on the hydrological observations of KJf (Iverson & Major, 1987; Schulz et al., 2018; Hahm et al., 2019 Finnegan et al., 2021).

To calibrate the model parameters for Boulder Creek and Mud Creek, we use the observed data from Minor Creek. We then adjusted the modeled landslide thickness for Minor Creek to back-calculate the hydraulic parameters required to match the observations assuming a 20 m thick (Mud Creek) and 40 m thick (Boulder Creek) landslide.

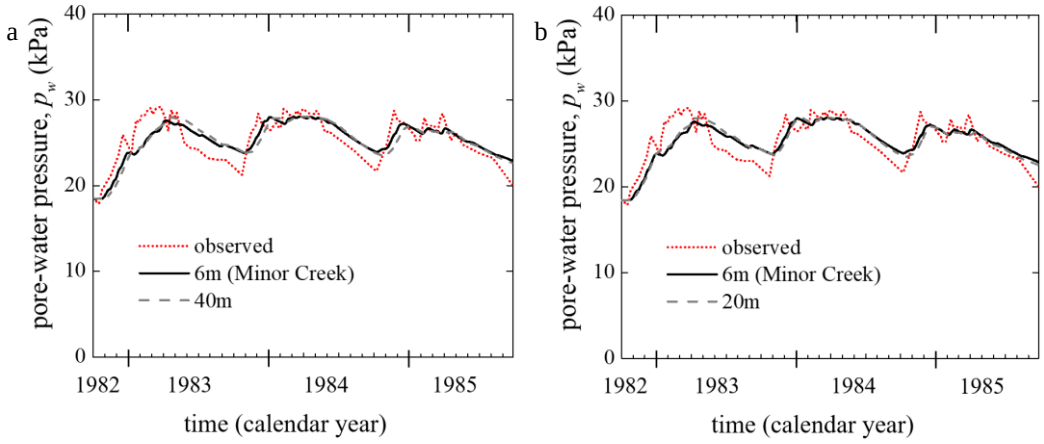

Figure A1. Calibration of Boulder Creek and Mud Creek hydraulic parameters. a) Simulation of Minor Creek with 40 m depth. b) Simulation of Minor Creek with 20 m depth.

Fig. A1a shows that when we change the thickness of Minor Creek to 40 m (i.e., Boulder Creek thickness), the k_s (saturated permeability) increases to 4.6E-6 m/s and S_s (storage coefficient) changes to 0.03 m^{-1} to simulate a similar hydrological response. Similarly, as depicted in Fig. A1b,

when we change the thickness of Minor Creek to 20 m (i.e., Mud Creek thickness) we must change the k_s 4.6E-6 m/s and S_s 0.07 m^{-7} to obtain a similar result. The deeper the infiltrated depth, the higher the diffusivity that is required to obtain the same hydrological response (Eq. 1).

Conflicts of interests

With the present all the authors declare that they do not have any financial and/or personal conflict with other people or organizations that could inappropriately influence or bias their work.

Sincerely yours,

Xiang Li

Alexander Handwerger

Giuseppe Buscarnera

Reference

Alonso, E., Zervos, A., & Pinyol, N. (2016). Thermo-poro-mechanical analysis of landslides: from creeping behaviour to catastrophic failure. *Géotechnique, 66*(3), 202-219.

Alonso, E. E., Gens, A., & Josa, A. (1990). A constitutive model for partially saturated soils. *Géotechnique, 40*(3), 405-430.

Angeli, M.-G., Gasparetto, P., Menotti, R. M., Pasuto, A., & Silvano, S. (1996). A visco-plastic model for slope analysis applied to a mudslide in Cortina d'Ampezzo, Italy. *Quarterly Journal of Engineering Geology and Hydrogeology, 29*(3), 233-240.

Augustesen, A., Liingaard, M., & Lade, P. V. (2004). Evaluation of time-dependent behavior of soils. *International Journal of Geomechanics, 4*(3), 137-156.

Bailey, E. H., Irwin, W. P., & Jones, D. L. (1964). *Franciscan and related rocks, and their significance in the geology of western California*. Retrieved from

Baum, R. L., & Reid, M. E. (1995). Geology, hydrology, and mechanics of a slow-moving. *Clay Shale Slope Instab, 10*, 79.

Bennett, G. L., Roering, J. J., Mackey, B. H., Handwerger, A. L., Schmidt, D. A., & Guillod, B. P. (2016). Historic drought puts the brakes on earthflows in Northern California. *Geophysical Research Letters, 43*(11), 5725-5731.

Berti, M., & Simoni, A. (2010). Field evidence of pore pressure diffusion in clayey soils prone to landsliding. *Journal of Geophysical Research: Earth Surface, 115*(F3).

Bingham, E. C. (1917). *An investigation of the laws of plastic flow*: US Government Printing Office.

Cascini, L., Calvello, M., & Grimaldi, G. M. (2010). Groundwater modeling for the analysis of active slow-moving landslides. *Journal of Geotechnical and Geoenvironmental Engineering, 136*(9), 1220-1230.

Cascini, L., Calvello, M., & Grimaldi, G. M. (2014). Displacement trends of slow-moving landslides: Classification and forecasting. *Journal of mountain science, 11*(3), 592-606.

Chen, Y., & Buscarnera, G. (2021). Numerical simulation of unstable suction transients in unsaturated soils: the role of wetting collapse. *International Journal for Numerical and Analytical Methods in Geomechanics, 45*(11), 1569-1587.

Chen, Y., & Buscarnera, G. (2022). Unified modeling framework of flowslide triggering and runout. Géotechnique, 1-37.

Cohen ‐ Waeber, J., Bürgmann, R., Chaussard, E., Giannico, C., & Ferretti, A. (2018). Spatiotemporal patterns of precipitation ‐ modulated landslide deformation from independent component analysis of InSAR time series. *Geophysical Research Letters, 45*(4), 1878-1887.

Conte, E., Donato, A., & Troncone, A. (2014). A finite element approach for the analysis of active slow-moving landslides. *Landslides, 11*(4), 723-731.

Corominas, J., Moya, J., Lloret, A., Gili, J., Angeli, M., Pasuto, A., & Silvano, S. (2000). Measurement of landslide displacements using a wire extensometer. *Engineering geology, 55*(3), 149-166.

Cui, Y., Jiang, Y., & Guo, C. (2019). Investigation of the initiation of shallow failure in widely graded loose soil slopes considering interstitial flow and surface runoff. *Landslides, 16*(4), 815-828.

di Prisco, C., & Imposimato, S. (1996). Time dependent mechanical behaviour of loose sands. *Mechanics of Cohesive‐frictional Materials: An International Journal on Experiments, Modelling and Computation of Materials and Structures, 1*(1), 45-73.

Di Toro, G., Hirose, T., Nielsen, S., Pennacchioni, G., & Shimamoto, T. (2006). Natural and experimental evidence of melt lubrication of faults during earthquakes. *Science, 311*(5761), 647-649.

Duncan, J. M. (1996). State of the art: limit equilibrium and finite-element analysis of slopes. *Journal of Geotechnical engineering, 122*(7), 577-596.

Fernández-Merodo, J. A., García-Davalillo, J., Herrera, G., Mira, P., & Pastor, M. (2014). 2D viscoplastic finite element modelling of slow landslides: the Portalet case study (Spain). *Landslides, 11*(1), 29-42.

Ferrari, A., Ledesma, A., González, D., & Corominas, J. (2011). Effects of the foot evolution on the behaviour of slow-moving landslides. *Engineering geology, 117*(3-4), 217-228.

Finnegan, N., Perkins, J., Nereson, A., & Handwerger, A. (2021). Unsaturated Flow Processes and the Onset of Seasonal Deformation in Slow‐Moving Landslides. *Journal of Geophysical Research: Earth Surface, 126*(5), e2020JF005758.

Hahm, W. J., Rempe, D. M., Dralle, D. N., Dawson, T. E., Lovill, S. M., Bryk, A. B., . . . Dietrich, W. E. (2019). Lithologically controlled subsurface critical zone thickness and water storage capacity determine regional plant community composition. *Water Resources Research, 55*(4), 3028-3055.

Handwerger, A. L., Huang, M.-H., Fielding, E. J., Booth, A. M., & Bürgmann, R. (2019). A shift from drought to extreme rainfall drives a stable landslide to catastrophic failure. *Scientific reports, 9*(1), 1-12.

Handwerger, A. L., Roering, J. J., & Schmidt, D. A. (2013). Controls on the seasonal deformation of slow-moving landslides. *Earth and Planetary Science Letters, 377*, 239-247.

Handwerger, A. L., Roering, J. J., Schmidt, D. A., & Rempel, A. W. (2015). Kinematics of earthflows in the Northern California Coast Ranges using satellite interferometry. *Geomorphology, 246*, 321-333.

Hendron Jr, A., & Patton, F. D. (1985). *The vaiont slide. A geotechnical analysis based on new geologic observations of the failure surface. Volume 1. Main text*. Retrieved from

Hilley, G. E., Bürgmann, R., Ferretti, A., Novali, F., & Rocca, F. (2004). Dynamics of slow-moving landslides from permanent scatterer analysis. *Science, 304*(5679), 1952-1955.

Hu, X., & Bürgmann, R. (2020). Rheology of a Debris Slide from the Joint Analysis of UAVSAR and LiDAR Data. *Geophysical Research Letters, 47*(8), e2020GL087452.

Hungr, O., Leroueil, S., & Picarelli, L. (2014). The Varnes classification of landslide types, an update. *Landslides, 11*(2), 167-194.

Hutchinson, J. (1986). A sliding–consolidation model for flow slides. *Canadian Geotechnical Journal, 23*(2), 115-126.

Iverson, R. M. (1985). Unsteady, nonuniform landslide motion: Theory and measurement.

Iverson, R. M. (2000). Landslide triggering by rain infiltration. *Water Resources Research, 36*(7), 1897-1910.

Iverson, R. M. (2005). Regulation of landslide motion by dilatancy and pore pressure feedback. *Journal of Geophysical Research: Earth Surface, 110*(F2).

Iverson, R. M. (2020). Landslide disparities, flume discoveries, and Oso despair. *Perspectives of Earth and Space Scientists, 1*(1), e2019CN000117.

669 Iverson, R. M., & Major, J. J. (1987). Rainfall, ground-water flow, and seasonal movement at
670 Minor Creek landslide, northwestern California: Physical interpretation of empirical
671 relations. *Geological Society of America Bulletin, 99*(4), 579-594.
672 Jennings, C. (1977). *GEOLOGIC MAP OF CALIFORNIA 1: 750 000*.
673 Keefer, D. K., & Johnson, A. M. (1983). *Earth flows; morphology, mobilization, and movement*
674 (2330-7102). Retrieved from
675 Kelsey, H., Coghlan, M., Pitlick, J., & Best, D. (1996). *Geomorphic analysis of streamside*
676 *landslides in the Redwood Creek basin, northwestern California.* Paper presented at the
677 International Journal of Rock Mechanics and Mining Sciences and Geomechanics
678 Abstracts.
679 Lacroix, P., Handwerger, A. L., & Bièvre, G. (2020). Life and death of slow-moving landslides.
680 *Nature Reviews Earth & Environment*, 1-16.
681 Leroueil, S. (2001). Natural slopes and cuts: movement and failure mechanisms. *Géotechnique,*
682 *51*(3), 197-243.
683 Li, D., Yan, L., Wu, L., Yin, K., & Leo, C. (2019). The Hejiapingzi landslide in Weining County,
684 Guizhou Province, Southwest China: a recent slow-moving landslide triggered by reservoir
685 drawdown. *Landslides, 16*(7), 1353-1365.
686 Li, X., Lizárraga, J. J., & Buscarnera, G. (2021). Regional-scale simulation of flowslide triggering
687 in stratified deposits. *Engineering geology, 292*, 106248.
688 Liingaard, M., Augustesen, A., & Lade, P. V. (2004). Characterization of models for time-
689 dependent behavior of soils. *International Journal of Geomechanics, 4*(3), 157-177.
690 Lizárraga, J. J., & Buscarnera, G. (2019). Spatially distributed modeling of rainfall-induced
691 landslides in shallow layered slopes. *Landslides, 16*(2), 253-263.
692 Mackey, B., Roering, J., & McKean, J. (2009). Long-term kinematics and sediment flux of an
693 active earthflow, Eel River, California. *Geology, 37*(9), 803-806.
694 Mackey, B. H., & Roering, J. J. (2011). Sediment yield, spatial characteristics, and the long-term
695 evolution of active earthflows determined from airborne LiDAR and historical aerial
696 photographs, Eel River, California. *Bulletin, 123*(7-8), 1560-1576.
697 Mansour, M. F., Morgenstern, N. R., & Martin, C. D. (2011). Expected damage from displacement
698 of slow-moving slides. *Landslides, 8*(1), 117-131.
699 Marinelli, F., Pisanò, F., Di Prisco, C., & Buscarnera, G. (2018). Model-based interpretation of
700 undrained creep instability in loose sands. *Géotechnique, 68*(6), 504-517.
701 Mitchell, J. K., Campanella, R. G., & Singh, A. (1968). Soil creep as a rate process. *Journal of the*
702 *Soil Mechanics and Foundations Division, 94*(1), 231-253.
703 Mizoguchi, K., Hirose, T., Shimamoto, T., & Fukuyama, E. (2007). Reconstruction of seismic
704 faulting by high‐velocity friction experiments: An example of the 1995 Kobe earthquake.
705 *Geophysical Research Letters, 34*(1).
706 Needleman, A. (1988). Material rate dependence and mesh sensitivity in localization problems.
707 *Computer methods in applied mechanics and engineering, 67*(1), 69-85.
708 Nereson, A., Davila Olivera, S., & Finnegan, N. (2018). Field and Remote‐Sensing Evidence for
709 Hydro‐mechanical Isolation of a Long‐Lived Earthflow in Central California.
710 *Geophysical Research Letters, 45*(18), 9672-9680.
711 Nereson, A. L. (2018). *History and Drivers of Slow Landslide Movement at Oak Ridge Earthflow,*
712 *California*: University of California, Santa Cruz.
713 Oberender, P. W., & Puzrin, A. M. (2016). Observation-guided constitutive modelling for creeping
714 landslides. *Géotechnique, 66*(3), 232-247.

Perzyna, P. (1963). The constitutive equations for rate sensitive plastic materials. *Quarterly of applied mathematics, 20*(4), 321-332.

Perzyna, P. (1966). Fundamental problems in viscoplasticity. In *Advances in applied mechanics* (Vol. 9, pp. 243-377): Elsevier.

Pisanò, F., & Prisco, C. d. (2016). A stability criterion for elasto‐viscoplastic constitutive relationships. *International Journal for Numerical and Analytical Methods in Geomechanics, 40*(1), 141-156.

Puzrin, A. (2012). *Constitutive modelling in geomechanics: introduction*: Springer Science & Business Media.

Puzrin, A. M., & Schmid, A. (2011). Progressive failure of a constrained creeping landslide. *Proceedings of the Royal Society A: Mathematical, Physical and Engineering Sciences, 467*(2133), 2444-2461.

Rice, J. R., Lapusta, N., & Ranjith, K. (2001). Rate and state dependent friction and the stability of sliding between elastically deformable solids. *Journal of the Mechanics and Physics of Solids, 49*(9), 1865-1898.

Richard, L. J. p. (1931). Capillary conduction of liquids through porous mediums. *1*(5), 318-333.

Roadifer, J. W., Forrest, M. P., & Lindquist, E. (2009). *Evaluation of shear strength of mélange foundation at Calaveras Dam.* Paper presented at the Proceedings of the 29th US Soc. for Dams, Annual Meeting and Conference:"Managing our Water Retention Systems", April.

Roering, J. J., Mackey, B. H., Handwerger, A. L., Booth, A. M., Schmidt, D. A., Bennett, G. L., & Cerovski-Darriau, C. (2015). Beyond the angle of repose: A review and synthesis of landslide processes in response to rapid uplift, Eel River, Northern California. *Geomorphology, 236*, 109-131.

Rutte, D., Garber, J., Kylander‐Clark, A., & Renne, P. R. (2020). An exhumation pulse from the nascent Franciscan subduction zone (California, USA). *Tectonics, 39*(10), e2020TC006305.

Scheingross, J. S., Minchew, B. M., Mackey, B. H., Simons, M., Lamb, M. P., & Hensley, S. (2013). Fault-zone controls on the spatial distribution of slow-moving landslides. *Bulletin, 125*(3-4), 473-489.

Schulz, W. H., Smith, J. B., Wang, G., Jiang, Y., & Roering, J. J. (2018). Clayey landslide initiation and acceleration strongly modulated by soil swelling. *Geophysical Research Letters, 45*(4), 1888-1896.

Sekiguchi, H. (1984). Theory of undrained creep rupture of normally consolidated clay based on elasto-viscoplasticity. *Soils and foundations, 24*(1), 129-147.

Shi, X. S., Herle, I., & Bergholz, K. (2017). A nonlinear Hvorslev surface for highly overconsolidated soils: elastoplastic and hypoplastic implementations. *Acta Geotechnica, 12*(4), 809-823.

Shi, Z., Hambleton, J. P., & Buscarnera, G. (2019). Bounding surface elasto-viscoplasticity: A general constitutive framework for rate-dependent geomaterials. *Journal of Engineering Mechanics, 145*(3), 04019002.

Skempton, A., & De Lory, F. (1957). Stability of natural slopes in London clay. *Thomas Telford Publishing, London, UK, 15*, 378-381.

Swain, D. L. (2021). A shorter, sharper rainy season amplifies California wildfire risk. *Geophysical Research Letters, 48*(5), e2021GL092843.

Taylor, W. L., & Pollard, D. D. (2000). Estimation of in situ permeability of deformation bands in porous sandstone, Valley of Fire, Nevada. *Water Resources Research, 36*(9), 2595-2606.

761 Terzaghi, K. (1925). Principles of soil mechanics. *Engineering News-Record, 95*(19-27), 19-32.
762 Tika, T. E., Vaughan, P., & Lemos, L. (1996). Fast shearing of pre-existing shear zones in soil.
763 *Géotechnique, 46*(2), 197-233.
764 Tschuchnigg, F., Schweiger, H., Sloan, S. W., Lyamin, A. V., & Raissakis, I. (2015). Comparison
765 of finite-element limit analysis and strength reduction techniques. *Géotechnique, 65*(4),
766 249-257.
767 Van Asch, T. W., Van Beek, L., & Bogaard, T. (2007). Problems in predicting the mobility of
768 slow-moving landslides. *Engineering geology, 91*(1), 46-55.
769 Veveakis, E., Vardoulakis, I., & Di Toro, G. (2007). Thermoporomechanics of creeping landslides:
770 The 1963 Vaiont slide, northern Italy. *Journal of Geophysical Research: Earth Surface,*
771 *112*(F3).
772 Wang, G., & Sassa, K. (2003). Pore-pressure generation and movement of rainfall-induced
773 landslides: effects of grain size and fine-particle content. *Engineering geology, 69*(1-2),
774 109-125.
775 Warrick, J. A., Ritchie, A. C., Schmidt, K. M., Reid, M. E., & Logan, J. (2019). Characterizing the
776 catastrophic 2017 Mud Creek landslide, California, using repeat structure-from-motion
777 (SfM) photogrammetry. *Landslides, 16*(6), 1201-1219.
778 Wedage, A., Morgenstern, N., & Chan, D. (1998). A strain rate dependent constitutive model for
779 clays at residual strength. *Canadian Geotechnical Journal, 35*(2), 364-373.
780 Wood, D. M. (1990). *Soil behaviour and critical state soil mechanics*: Cambridge university press.
781 Yeh, G., & Ward, D. (1980). *FEMWATER: A finite-element model of water flow through*
782 *saturated-unsaturated porous media*. Retrieved from
783 Zambelli, C., Di Prisco, C., & Imposimato, S. (2004). A cyclic elasto-viscoplastic constitutive
784 model: theoretical discussion and validation. *Cyclic Behaviour of Soils and Liquefaction*
785 *Phenomena*, 99-106.

786